Accepted Manuscript

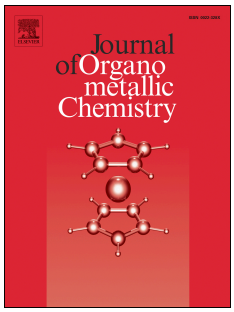

On the structure of *meso*-substituted F-BODIPYS and their assembly in molecular crystals: An experimental-theoretical approach

Elba Xochitiotzi-Flores, Alisul A. Islas-Mejia, Héctor García-Ortega, Margarita Romero-Ávila, José Manuel Mendez-Stivalet, María del Pilar Carreón-Castro, Rosa Santillan, Mauricio Maldonado-Domínguez, Rafael Arcos-Ramos, Norberto Farfán

PII: S0022-328X(16)30021-3

DOI: 10.1016/j.jorganchem.2016.01.021

Reference: JOM 19372

To appear in: *Journal of Organometallic Chemistry*

Received Date: 10 November 2015

Revised Date: 11 January 2016

Accepted Date: 13 January 2016

Please cite this article as: E. Xochitiotzi-Flores, A.A. Islas-Mejia, H. García-Ortega, M. Romero-Ávila, J.M. Mendez-Stivalet, M.d.P. Carreón-Castro, R. Santillan, M. Maldonado-Domínguez, R. Arcos-Ramos, N. Farfán, On the structure of *meso*-substituted F-BODIPYS and their assembly in molecular crystals: An experimental-theoretical approach, *Journal of Organometallic Chemistry* (2016), doi: 10.1016/j.jorganchem.2016.01.021.

Graphical Abstract

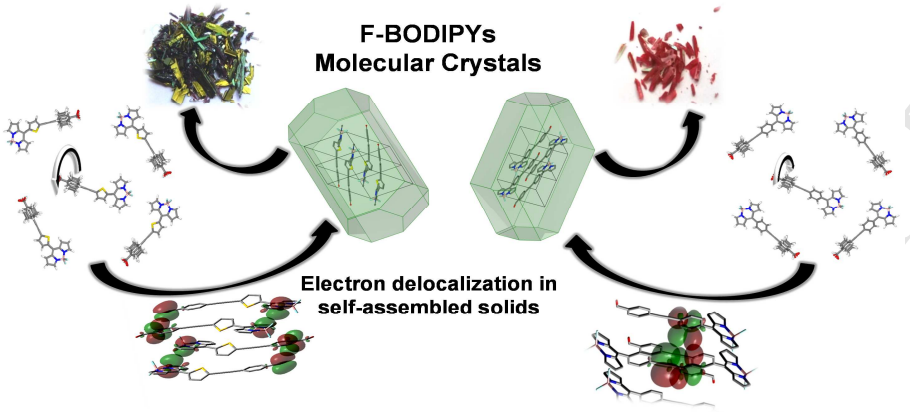

On the structure of *meso*-substituted F-BODIPYS and their assembly in molecular crystals: An experimental-theoretical approach

Elba Xochitiotzi-Flores,[a] Alisul A. Islas-Mejia,[a] Héctor García-Ortega,[a] Margarita Romero-Ávila,[a] José Manuel Mendez-Stivalet,[a] María del Pilar Carreón-Castro,[c] Rosa Santillan,[b] Mauricio Maldonado-Domínguez,[a] Rafael Arcos-Ramos,[c] Norberto Farfán[a]*

[a] Facultad de Química, Departamento de Química Orgánica, Universidad Nacional Autónoma de México, 04510 México D.F., México. E-mail: norberto.farfan@gmail.com

[b] Departamento de Química, Centro de Investigación y de Estudios Avanzados del IPN, México D.F. Apdo. Postal 14-740, 07000, México

[c] Departamento de Química de Radiaciones y Radioquímica, Instituto de Ciencias Nucleares, Universidad Nacional Autónoma de México, 04510 México D.F., México. E-mail: rafaelarcos84@gmail.com

Introduction

The possibility to tailor fluorescent small-molecular compounds to display predefined features has been very useful for medicinal, molecular and materials applications. The progress in fluorescence and microscopy imaging techniques is intimately related to the evolution of dyes and small-molecular fluorophores. In this sense, 4,4-difluoro-4-bora-3a,4a-diaza-*s*-indacene derivatives (*see* Figure 1), typically named F-BODIPYs, have received particular attention due to their absorption and emission profiles, along with synthetic feasibility and chemical stability [1]. F-BODIPYs have been tested in DNA sequencing and bio-analysis [2], as fluorescent probes [3], as molecular sensors [4], in photodynamic therapy [5], and in organic light emitting diodes (OLEDs) [6]. Moreover, it is possible to tune their spectroscopic and photo-physical properties functionalizing the pyrrole core, the *meso* position and also the boron substituents, depending on the properties and the applications to achieve [7].

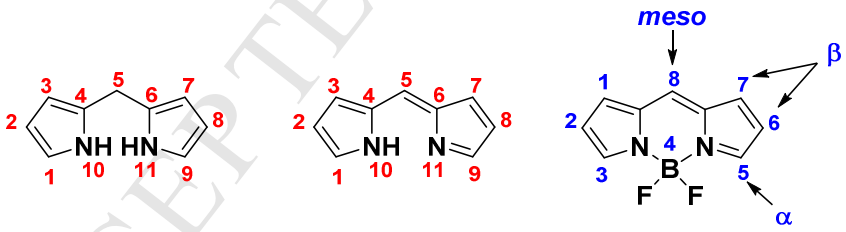

Figure 1. Generic structural formulas for: dipyrromethane, dipyrromethene, and F-BODIPY cores.

In general, there are various strategies to functionalize the F-BODIPY dyes at the *meso*-position. Particularly, the *meso*-aryl F-BODIPYs are readily prepared from commercial aromatic aldehydes; in this case, the *meso*-aryl substituent adopts an orthogonal

conformation with respect to the F-BODIPY core which reflects in suboptimal electronic coupling between them. Alternatives to introduce substituents *via* nucleophilic aromatic substitution or by palladium-catalyzed cross-coupling reactions at *meso*-position are the use of *meso*-methylthio-F-BODIPYs [8] or *meso*-halogenated-F-BODIPYs [9]. Another strategy involves the introduction of electron-donor groups at *meso*-position bridged by an ethynyl group, which favors electronic coupling between the introduced substituent and the F-BODIPY core [10].

In contrast with these rotationally-unhindered systems, where molecular response to absorption may be fine-tuned by remote functionalization at the incorporated moiety, *meso*-aryl substituents display only very small responses to functional group introduction or structural decoration at distal positions. Due to sterically-hindered planarization, absorption and fluorescence bands arise mainly from transitions within the BODIPY core; only minute contribution from the staggered, vicinal aryl group are observed; electron-donor groups directly attached to this *meso*-position, however, have been found to significantly blue-shift absorption and emission maxima [11]. On the other hand, electron-acceptor substituents red-shift the spectral characteristics of the BODIPY core [12]. An appealing feature of *meso*-aryl F-BODIPYs is, hence, their potential application as molecular tags, whose introduction into larger systems embodied this partial disruption of π-electron delocalization, isolating the F-BODIPY core, and its properties as chromophore, from remote electronic effects.

Generally, the photophysics of F-BODIPYs is insensitive to solvent effects; *meso*-substitution with the adequate electron-donor or acceptor groups provokes, however, different photophysical processes in response to the environment. To achieve an efficient light-harvesting system, covering the broadest region within the visible spectrum, the

adequate combination of electron-donor and electron-acceptor groups substituting the *meso*-position and F-BODIPY core must be met. Regrettably, detailed analysis about the influence of single substituents on the absorption and emission of these kinds of dyes is not present in the literature.

Herein we report a synthetic route to obtain highly crystalline F-BODIPYs. These compounds display a reactive formyl group for covalent anchoring and derivatization. Through carbonyl chemistry, a wide chemical space may be readily covered, giving access to a diverse palette of increasingly-complex systems; introduction of molecular antennae to different structures may be performed as well. To delve deeper into the structural and electronic properties of the molecular crystals based on F-BODIPYs, the featured molecular structures were thoroughly studied using an experimental-theoretical approach. Electronic excitations were characterized for the highlighted compounds through UV-Vis and time-dependent density-functional-theory (TDDFT) studies. The different degrees of electronic communication and conformational freedom were studied through this tandem strategy to describe the absorptive behavior of these chromophores in solution. The presented molecules readily provided molecular crystals which were solved within the P-1 group. Solid-state superstructures exhibited periodic networks of directionally-stacked subunits, as derived through analysis of the computed electron density for each experimental unit-cell within the Quantum Theory of Atoms in Molecules (QTAIM). Natural Bonding Orbitals (NBO) computed for these densities feature in-phase intermolecular overlap across the molecular crystal, evidencing electronic communication among molecules within the crystalline domain. CASTEP analysis of the periodic lattices suggests a semiconductor character for both molecular crystals.

Results and Discussion

*Synthesis and structural characterization of F-BODIPYs **4a-b**.*

The F-BODIPYs **2a-b** were synthesized in good yields following classical methodologies reported for these compounds (see Supporting Information File), the spectroscopic data confirmed their presence and matched with the previously reported [13]. The brominated F-BODIPYs **2a-b** were reacted with 4-ethynylbenzaldehyde **3** under Pd(0)-catalyzed Sonogashira cross-coupling conditions [14] to produce the corresponding F-BODIPYs **4a** (80 %) and **4b** (63 %) in moderate yields (*see* Scheme 1).

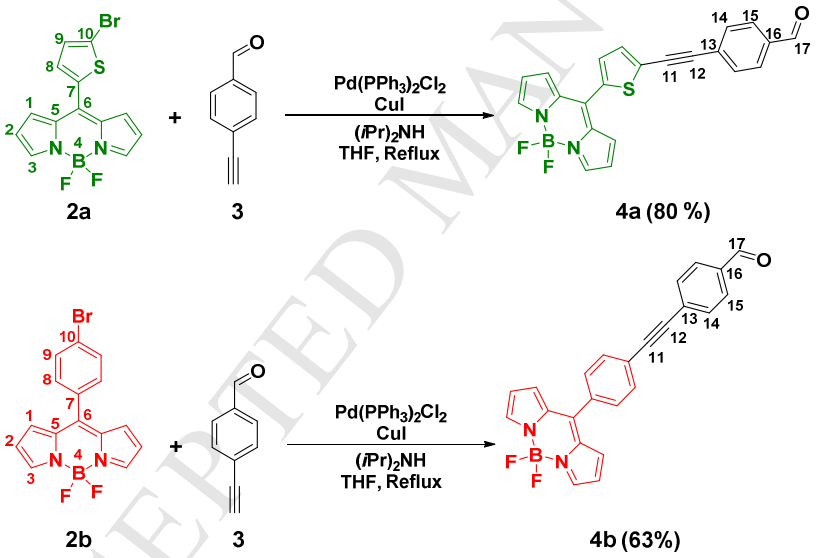

Scheme 1. Synthesis of F-BODIPYs **4a-b**.

The synthesis of F-BODIPYs was corroborated by solution NMR experiments, where the ^{1}H-NMR spectrum of **4a** showed a single signal at δ = 10.04 ppm for (H-17) and two doubles signals at δ = 7.90 (H-15) and 7.70 ppm (H-14), confirming the presence of the benzaldehyde fragment. The thiophene ring displayed two doublet signals at δ = 7.50 (H-9)

and 7.45 ppm (H-8). In the ^{1}H-NMR spectrum of **4b**, the aldehyde hydrogen appeared as a single signal at δ = 10.05 ppm (H-17). The phenyl rings can be unambiguously distinguished: the two doublets at δ = 7.91 (H-15) and 7.60 ppm (H-14) for the benzaldehyde fragment, and the doublet-doublet-doublet signal at δ = 7.72 ppm (H-8, H-9) for the phenyl bridge. The characteristic signals for the benzaldehyde fragment at δ = 191.2 (C-17), 136.0 (C-16), 132.0 (C-14), 129.7 (C-15), 128.2 ppm (C-13) for **4a** and 191.5 (C-17), 135.9 (C-16), 130.7 (C-14), 129.8 (C-15) and 125.4 ppm (C-13) for **4b,** were present in the ^{13}C-NMR spectra. The alkyne bridge appeared at δ = 96.0, 91.2 (C-12) and 85.2, 92.1 ppm (C-11) for **4a** and **4b**, respectively. Evidence for the boron complexation was obtained through ^{11}B- and ^{19}F-NMR experiments; for both compounds, a triple signal appeared *ca.* δ = -0.27 ppm, and a quartet at *ca.* δ = -145 ppm, respectively. The observed peaks at *m/z* 403.0889 (**4a**) and 397.1321 (**4b**) from high resolution mass spectrometry analyses were in accordance with the expected molecular ions. The FTIR spectra for F-BODIPYs **4a-b** showed the characteristic band for the C=O stretch at *ca*. ν = 1699 cm^{-1}, and the band for the -C≡C- stretching around ν = 2200 cm^{-1} for both compounds.

Suitable single crystals for X-Ray diffraction of compound **4a** were grown by slow evaporation of acetone solutions in partially closed glass vials. The molecular structure of compound **4a** was solved in the triclinic space group P-1 with Z = 2 as shown in Figure 2a.

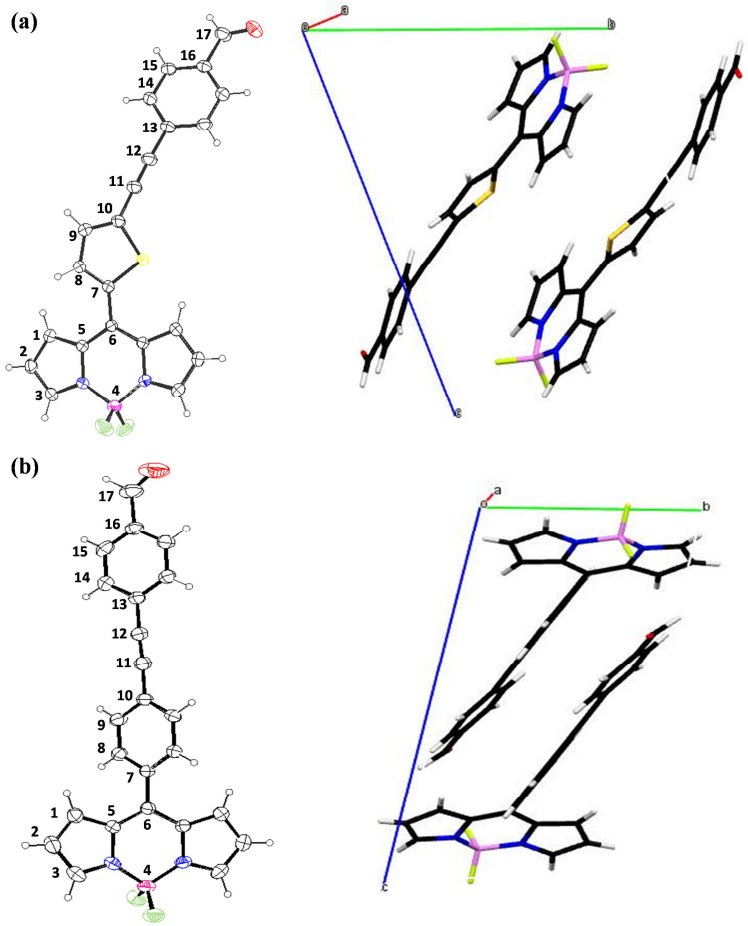

Figure 2. ORTEP diagrams with atom numbering for F-BODIPYs (a) **4a** and (b) **4b**. Thermal ellipsoids are drawn at 30 % probability level for all atoms other than hydrogen; their corresponding unit cells are viewed along the crystallographic *a* axis.

The structure of **4a** in the crystalline phase is not planar; the values of dihedral angles, discussed below confirmed this statement. Hydrogen-bonding C2-H2···O1 (**2.64 Å**) and C14-H14···F1 (**2.68 Å**) interactions aligned the molecules in a *head to tail* fashion creating one-dimensional monolayers. These monolayers are self-assembled by complementary hydrogen-bonding interactions between the BODIPY cores, C3-H3···F1 (**2.54 Å**) and C3'-H3'···F2 (**2.47 Å**) (see Figure 3).

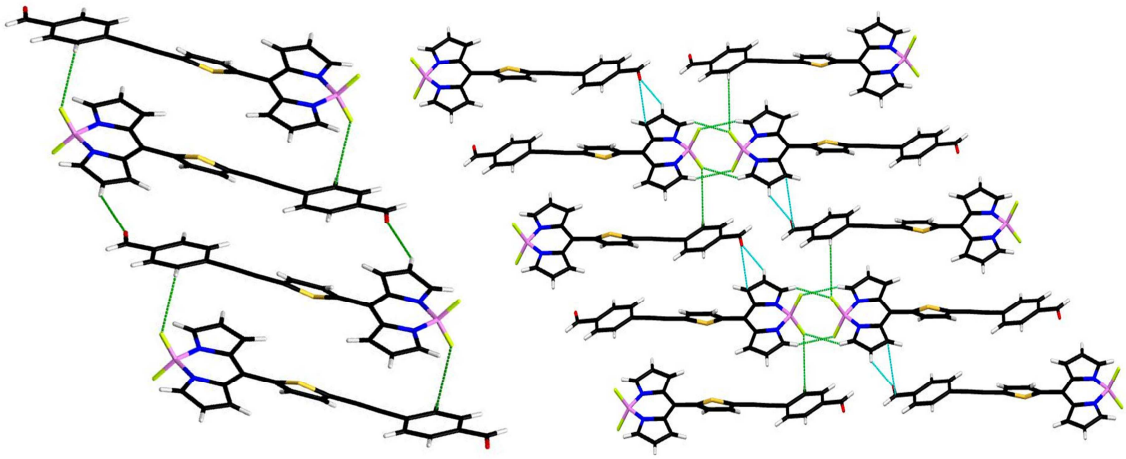

Figure 3. Crystal packing displayed by F-BODIPY **4a**. The pictures are viewed along the crystallographic *a* axis.

Dihedral angles between selected planes: (1) BODIPY core, (2) aryl *meso*-substituent and (3) benzaldehyde ring are calculated using all non-hydrogen atoms through the graphical interface from SHELXL [15] and Mercury [16] programs; the results are summarized in table 1. The dihedral angle values were 44 ° for **4a** and 55 ° for **4b** between planes 1 and 2, the result for **4a** is reasonable considering hindrance arising from a single H-H interaction and a, presumably favorable, H-S contact; the larger value for **4b** is expected for hindered rings (such as 85 ° for *o*-tolyl or 75° for mesityl *meso*-substituents), due to restricted motion around the pyrrole rings [17]. Obviously, smaller values for dihedral angles between the BODIPY core and aryl *meso*-substituents are expected to favor electron density delocalization over the π-conjugated system.

Compound	Mean Planes	Dihedral angle (°)
4a	1-2	44.0
	1-3	17.6
	2-3	37.9
4b	1-2	55.3
	1-3	45.4
	2-3	9.9

Table 1. Selected dihedral angles (°) in F-BODIPYs **4a-b.**

Crystals of F-BODIPY **4b** were obtained by slow evaporation of hexanes/methylene chloride solutions (3:2) in partially closed glass vials. In a similar manner to compound **4a**, the molecular structure of F-BODIPY **4b** was solved in the triclinic P-1 space group with Z = 2 (Figure 2b). Again, the dihedral angles values demonstrated the non-planarity of the system. The molecules of F-BODIPY **4b** are held together by hydrogen-bonding C1-H1···O1 (**2.48Å**) and C8-H8···F1 (**2.66 Å**) interactions in a *head to tail* manner as shown in figure 4.

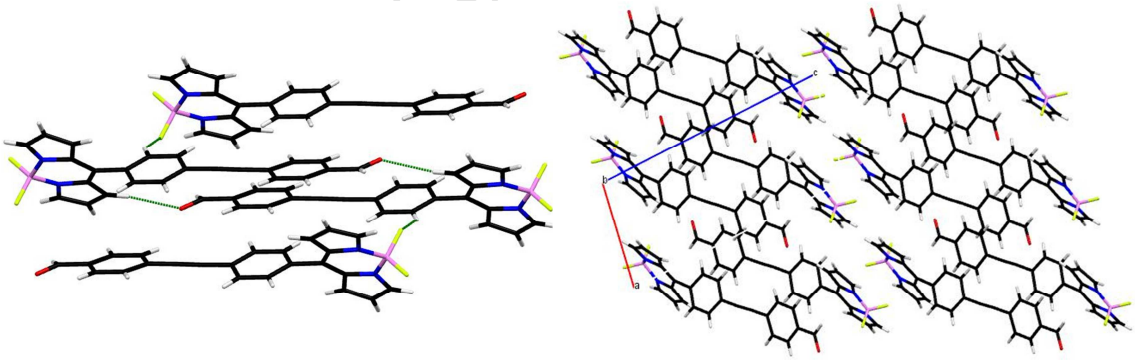

Figure 4. Crystal packing displayed by F-BODIPY (**4b**). The pictures are viewed along the crystallographic *a* axis.

The characteristic bond lengths in F-BODIYs **4a-b**, N(1)-B, N(1')-B, B-F(1), B-F(1'), C(5)-C(6), C(5')-C(6), C(5)-N(1) and C(5')-N(1') (see Supporting Information File) are in the same range of analogous F-BODIPYs. Specially, the bond distance C(6)-C(7) for **4b** [1.478 (3) Å] is in accordance with values previously reported for several *meso*-aryl substituted F-BODIPYs [17-18]. In the case of F-BODIPY **4a**, a shorter bond distance [1.466 (3) Å] compared with **4b** was found, which is in good agreement with reported data for *meso*-thiophenyl substituted F-BODIPYs [19].

*Spectroscopic properties and TDDFT studies for F-BODIPYs **4a-b***

The F-BODIPYs **4a** and **4b** were studied through UV-Vis spectroscopy. The absorption profile for these compounds is shown in figure 5; it features a set of multiple excitations accessible at room temperature within the studied wavelength range.

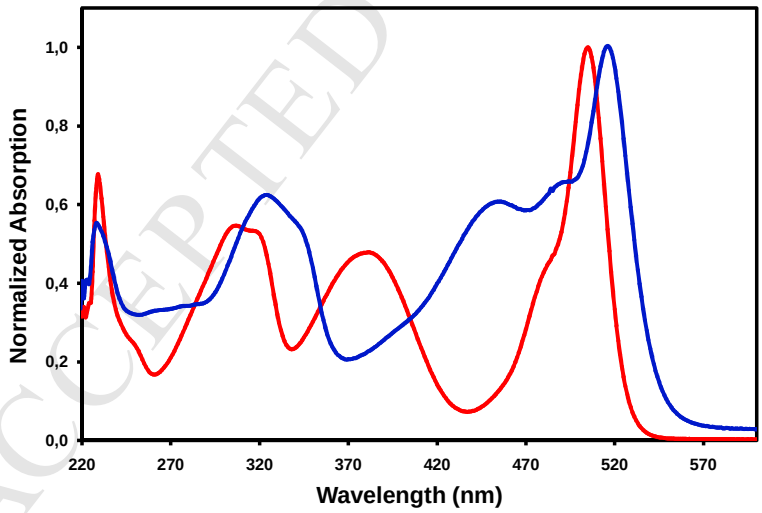

Figure 5. UV-Vis absorption profiles for compounds **4a** (blue) and **4b** (red), recorded from 1 x 10^{-5} M solutions in chloroform.

Time-dependent density functional theory (TDDFT) studies have been previously applied to describe the electronic transitions in UV-Vis spectroscopy of F-BODIPYs derivatives [20]. The absorption spectra of compounds **4a-b** were analyzed and the observed excitations assessed using the PW91 functional with the DNP+ numerical basis set [21], using the COSMO model for implicit solvation in chloroform [22].

For compound **4a**, an intense absorption band at 518 nm is observed, due to a π-π* transition involving the BODIPY core and an average contribution from rotamers in solution. To approach a qualitative description of this phenomenon, a static scan of the conformational subspace derived from rotation of the remote benzaldehyde moiety was performed and the results are shown in figure 6.

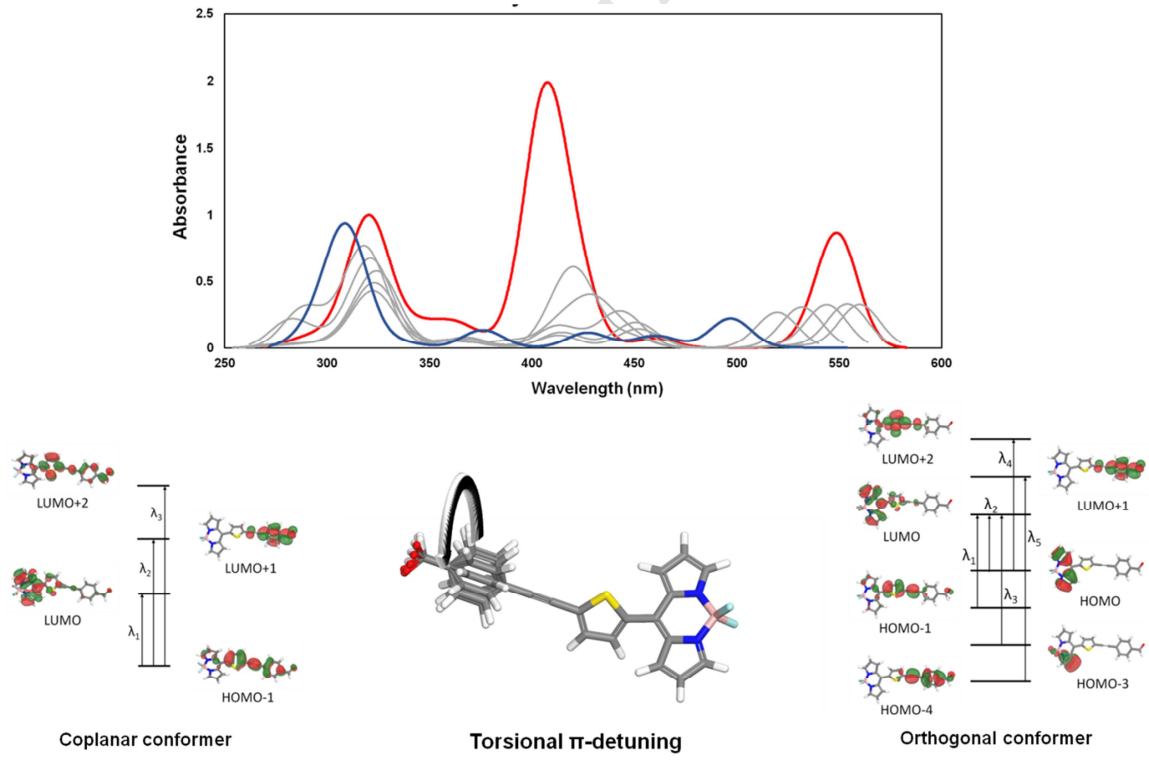

Figure 6. Torsion-dependent absorbance, computed through TDDFT at the PW91/DNP+ level for F-BODIPY **4a** in chloroform, using the COSMO solvation scheme. This shows

the theoretical effect of detuning the benzaldehyde moiety from coplanarity (red plot) to orthogonality (blue plot). Gray curves represent intermediate conformational states derived from π-detuning in stepwise 15° torsions.

As can be seen under this approximation, the available electronic transitions are expected to change substantially upon rotation of the alkyne bridge. It is clear, however, that the lowest-energy excitation is, consistently, arising from π-density polarization within the F-BODIPY core, coupled to the neighboring π-subsystem as a function of conformational state. Two additional, well-resolved absorptions may be observed in the experimental spectrum of **4a**. According to TDDFT, these correspond with π-π* transitions involving a) excitation of the thiophene-alkyne-benzaldehyde, a donor-bridge-acceptor π-subsystem and b) a local excitation of the 4-substituted benzaldehyde moiety.

In the case of F-BODIPY **4b**, the most intense absorption band appeared experimentally at 506 nm. Again, this signal corresponds to the F-BODIPY core, while the additional bands arise, according to computation, are due to excitation of the phenylene-alkyne-benzaldehyde system, as shown in figure 7, in a manner analogous to that of compound **4a**.

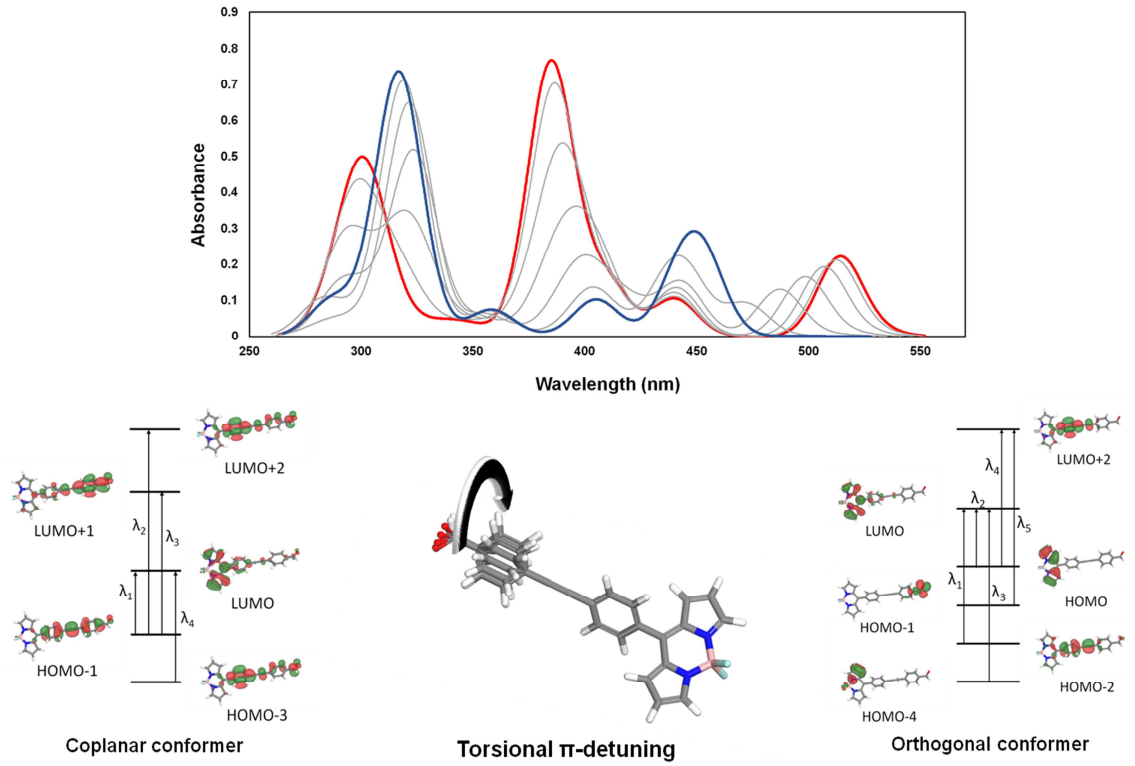

Figure 7. Torsion-dependent absorbance, computed through TDDFT at the PW91/DNP+ level for F-BODIPY **4b** in chloroform, using the COSMO solvation scheme. This shows the theoretical effect of detuning the benzaldehyde moiety from coplanarity (red plot) to orthogonality (blue plot). Gray curves represent intermediate conformational states derived from π-detuning in stepwise 15° torsions.

*Theoretical studies of molecular crystals from F-BODIPYs **4a-b***

Analysis of the electron density for the crystal structure of **4a** through AIM theory provided the bonding-paths shown in figure 8 [23]. Intermolecular contacts among π systems are observed across the stacked network, along with computed favorable π-H dispersive interactions intercommunicating vicinal layers. The lack of axial symmetry within the thiophene moiety reflects in alternation in the layered structure of this molecular crystal which, if decomposed into stacked subsystems, features BODIPY-BODIPY contacts

among parallel structures within a single layer, while BODIPY-bridge bond paths interconnect antiparallel, neighboring layers.

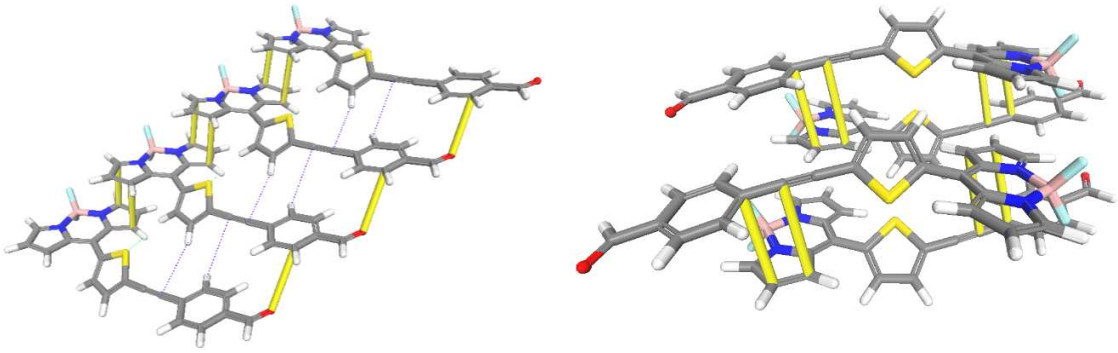

Figure 8. The framework of cooperative π-interactions, computed through DFT-AIM, for the periodic structure derived from SXRD of compound **4a**. The contacts contributing to (right) intralayer and (left) interlayer cohesion are depicted as yellow bars. Selected dispersive contacts are illustrated as dashed blue lines. For the full BCP network, please refer to supplementary information file.

From a natural bonding orbital perspective, donor-acceptor pairs manifest across the network of directly π-stacked molecular units. When observing the corresponding natural bonding orbitals, distance and directionality contribute to a predicted overlap among N-C π systems, with in-phase overlap within this donor-acceptor pair. An *n*-π contact is suggested by a bond path interconnecting the oxygen atom and a neighboring phenyl ring. As shown in figure 9, this contact is out of range for orbital overlap, as computed by NBO. Thus, local dipolar or dispersive interactions may be invoked for this bond critical point and its associated interbasin path. Electrostatic potential isosurfaces computed for these supramolecules depicts zones of negative charge interconnecting molecular subunits; these can be ascribed to the predicted in-phase orbital contacts.

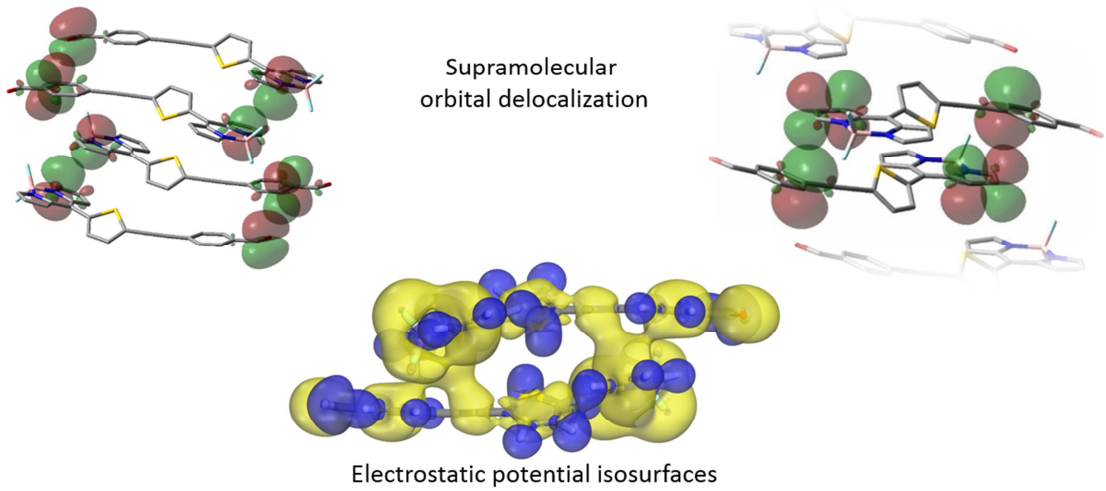

Figure 9. In the NBO picture for the molecular crystal of compound **4a**, in-phase contacts among dimeric subunits are expected between F-BODIPY cores. Benzaldehyde moieties display no additive overlap, so interaction between these centers may be regarded as an electrostatic/VdW contact. Surfaces computed at the HF 6-31G(d) level. ESP surfaces illustrate the effect of delocalization on net charge distribution. Yellow and blue colors indicate negative and positive ESP, respectively.

The relatively rigid structure of these compounds, coupled to their π electron density, result in cooperative π interactions. This picture may be inferred from the crystal packing in figures 3-4. The framework of overlapping systems in molecular crystal **4b** is shown in figure 10, along with the analysis of electron density through Atoms-in-Molecules Quantum Theory.

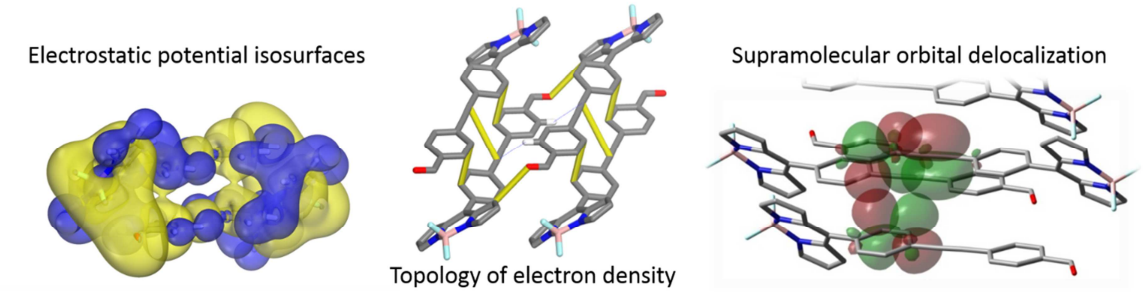

Figure 10. Framework of cooperative π-interactions (DFT-AIM), electrostatic potential maps (ESP) and orbital contacts between molecular subunits within the crystal structure of compound **4b** (NBO, HF/6-31G(d)). Relevant hydrogen atoms included for clarity. For the full BCP network, please refer to supplementary information file. Yellow and blue colors indicate negative and positive ESP, respectively.

As can be seen, intermolecular contacts occur between atomic basins with π-electron density. The exhibited directionality suggests a periodic stacking with branching points converging at the alkyne bridge. Natural Bonding Orbitals [24], derived for this system show complex delocalized motifs across the experimental lattice. The diffuse π density around the alkyne bridge (a donor) establishes contact with two neighboring, mutually-contacting benzene rings (acceptors). The overall interaction delocalizes electron density in an intermolecular fashion. It is noteworthy that, in contrast with the molecular crystal derived from **4a**, no π-overlap is foreseen between parallel subunits.

This study gives an insight into the nature of the interactions involved in the solid-state structure of the obtained molecular crystals. Stacking manifested throughout analysis, playing a key structural role through the establishment of a periodic net of overlapping electron density. The bonding character of this orbital overlap, along with a set of

dispersive contacts, dipole cancellation, hydrogen-bonds, contributed cooperatively to crystalline self-assemblage, in accordance with previous reports [10b, 25].

*CASTEP analysis of the molecular crystals from F-BODIPYs **4a** and **4b***

Partial density of states (PDOS) for the studied molecular crystals was derived through a semiempirical DFT approach with the plainwave-based CASTEP code, implemented within MS8 [26]. PDOS diagrams are presented in figure 11, decomposing full DOS into atomic contributions.

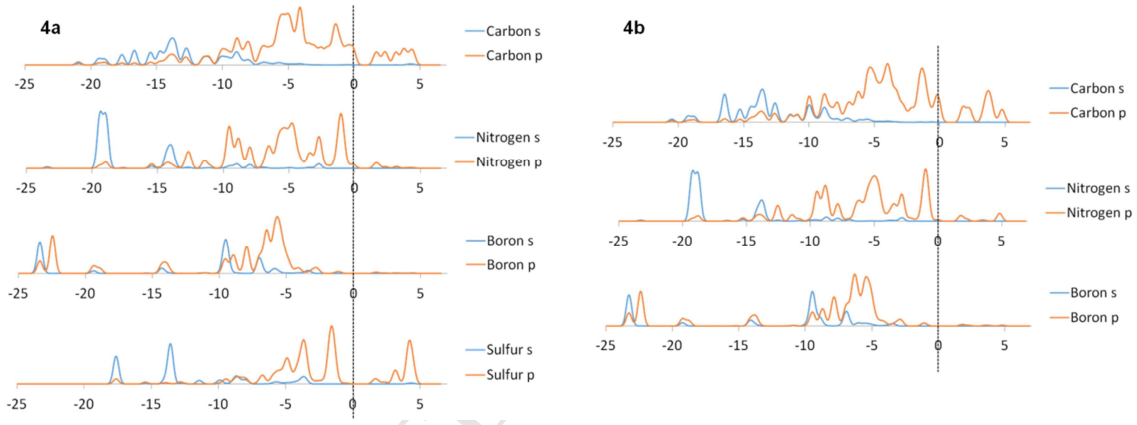

Figure 11. Partial density of states for compounds **4a** and **4b**, computed with the PW91 functional with norm conserving pseudopotential. The Fermi level is set to 0 eV.

Density of states for both molecular crystals suggests, in concordance with the natural orbital description, a high contribution from carbon and nitrogen to the top valence bands (represented by the highest density of states near the Fermi level), with a dominant p-character for both PDOS involved in delocalization. Additionally, the soft carbon p-component in predicted to account for most of the conduction bands in both **4a** and **4b**

crystals. In the molecular crystal of **4a**, sulfur PDOS exhibits important contributions to this conduction band, thus pointing towards a periodic effect in electron-density distribution derived from the thiophene moiety. The corresponding results for boron PDOS in both crystals imply it does not contribute to periodic delocalization of electron density. The hard character of boron manifests in this fashion, being electronically-isolated within the BODIPY core.

Conclusions

In this work, two F-BODIPYs **4a-b** have been synthesized and characterized using an experimental-theoretical approach. The F-BODIPYs were prepared using Pd(0)-catalyzed Sonogashira cross-coupling reactions and their molecular structures were studied starting from the molecular crystal coordinates which were solved in the P-1 space group. These chromophores feature carboxaldehyde groups for covalent attachment to systems of interest as molecular antennae. Due to their versatility, these functionalities allow for further increase in molecular complexity, thus giving access to a wide chemical space for potential applications in materials science, photochemistry and photophysics with absorption-emission profiles characterized and analyzed through TDDFT.

Single crystals were obtained for both compounds, and analyzed through a SXRD-NBO-QTAIM-CASTEP strategy. The crystalline lattices display in-phase, intermolecular π-contacts among molecular subunits, delocalizing electron density through periodic stacking and further stabilizing the solid network through dispersive Van der Waals interactions. Partial density of states suggests a semiconductor character for both molecular crystals, with an important contribution from carbon p-density to top valence and bottom conduction

bands. An additional contribution arising from sulfur is predicted for thiophene-containing compound **4a**, suggesting a higher degree on intermolecular delocalization in the corresponding molecular crystal.

Materials and Methods

Synthesis and characterization

General

All the reactions were carried out under a nitrogen atmosphere. The starting materials were purchased from commercial sources and used as received without further purification. Tetrahydrofuran (THF) was distilled from sodium-benzophenone in a continuous still under a nitrogen atmosphere. CH_2Cl_2 was dried over calcium hydride prior to use. Pyrrole was distilled before use. Reactions were monitored by analytical thin layer chromatography (TLC) on pre-coated silica gel plates (ALUGRAM SIL G/UV_{254}) revealed by exposure to a UV_{254} lamp. Flash column chromatography was performed using silica gel (230-400 mesh) as the stationary phase.

Physical measurements

Melting points were measured in a Barnstead Electrothermal 9300 apparatus and are uncorrected. FTIR experiments were recorded in a Perkin-Elmer Spectrum 400 FTIR/FT-FIR and Shimadzu FTIR-ATR-8300 spectrophotometers as solid samples using Attenuated Total Reflectance. NMR experiments were recorded in $CDCl_3$ solution in a Varian Unity Inova 400, JEOL Eclipse 400 and Bruker ARX 300 spectrometers, all the chemical shifts are reported in ppm with respect to TMS using residual solvent as reference, fixed on δ =7.26 ppm for ^1H, δ = 77.00 ppm for ^{13}C. Boron NMR spectra were referenced to external $BF_3 \cdot Et_2O$ in $CDCl_3$ set as 0 ppm. Fluorine NMR spectra were referenced to $CFCl_3$

set as 0 ppm. The coupling constants (*J*) are reported in Hz, multiplicities signals are reported as: singlet (s), broad (br), doublet (d), doublet-doublet (dd), doublet-doublet-doublet (ddd), triplet (t), quartet (q), multiplet (m). High Resolution Mass Spectrometry (HRMS) data were acquired in an Agilent Technologies MS TOF spectrometer. Mass spectra were obtained from a Thermo-Electron DFS spectrometer instrument by electron impact (EI) ionization technique. Elemental Analysis was recorded on Perkin Elmer 2400, using as calibration compound Cysteine.

Synthesis of *meso*-(5-((4-formylphenyl)ethynyl)thiophen-2-yl)-4,4-difluoro-4-bora-3a,4a-diaza-s-indacene (F-BODIPY 4a). To a solution of F-BODIPY **2a** (0.65 g, 1.85 mmol), $Pd(PPh_3)_2Cl_2$ (0.07 mg, 0.09 mmol) and CuI (0.02 mg, 0.09 mmol) in anhydrous THF (40 mL) under nitrogen atmosphere, were added dropwise $(i\text{Pr})_2\text{NH}$ (0.80 mL, 5.55 mmol) and 4-ethynylbenzaldehyde **3** (0.24 g, 1.85mmol) in THF (10 mL). The reaction mixture was heated to reflux for 4 h. After this time, the reaction was quenched with saturated solution of NH_4Cl and extracted with CH_2Cl_2. The organic phase was dried over anhydrous Na_2SO_4 and the solvent was evaporated to dryness under vacuum. The crude product was purified by flash chromatography using hexanes/acetone (90:10) as eluent to afford F-BODIPY **4a** as green metallic solid (**0.60 g, 80 %**). Melting point (°C): 156-158. FTIR (ATR) (ν, cm^{-1}): 3109, 2200, 1698, 1536, 1417, 1387, 1255, 1111, 1067, 1025, 972, 820, 774, 729. UV-Vis ($CHCl_3$) λ = 325, 447, 518 nm. ^{1}H-NMR [400 MHz, $CDCl_3$] (δ, ppm): 10.04 (s, 1H, H-17), 7.95 (br, 2H, H-3), 7.90 (d, *J* = 8.4 Hz, 2H, H-15), 7.70 (d, *J* = 8.4 Hz, 2H, H-14), 7.49 (d, *J* = 4.0 Hz, 1H, H-9), 7.45 (d, *J* = 4.0 Hz, 1H, H-8), 7.29 (d, *J* = 4.3 Hz, 2H, H-1), 6.60 (dd, *J* = 4.3, 1.3 Hz, 2H, H-2). ^{13}C-NMR [100 MHz, $CDCl_3$] (δ, ppm): 191.2 (C-17), 144.3 (C-3), 138.0 (C-7), 136.4 (C-5), 136.0 (C-16), 134.2 (C-6),

133.4 (C-9), 132.8 (C-8), 132.0 (C-14), 131.3 (C-1), 129.7 (C-15), 128.5 (C-10), 128.2 (C-13), 118.8 (C-2), 96.0 (C-12), 85.2 (C-11). ^{11}B-NMR [128.3 MHz, $CDCl_3$] (δ, ppm): -0.26 (t, *J* = 28.6 Hz). ^{19}F-NMR [282.4 MHz, $CDCl_3$] (δ, ppm): -145.17 (q, *J* = 28.6 Hz). HRMS calculated for *m/z* $C_{22}H_{13}BF_2N_2OS+H^+$ 403.0888, found 403.0889.

Synthesis of *meso*-(4-((4-formylphenyl)ethynyl)phenyl)-4,4-difluoro-4-bora-3a,4a-diaza-*s*-indacene (F-BODIPY 4b). To a solution of F-BODIPY **2b** (0.50 g, 1.45 mmol), $Pd(PPh_3)_2Cl_2$ (0.05 g, 0.07 mmol) and CuI (0.02 g, 0.07 mmol) in anhydrous THF (40 mL) under nitrogen atmosphere, were added dropwise $(i\text{Pr})_2\text{NH}$ (0.60 mL, 4.36 mmol) and 4-ethynylbenzaldehyde **3** (0.19 g, 1.45 mmol) in THF (10 mL). The reaction mixture was heated to reflux for 4 h. After this time, the reaction was quenched with saturated solution of NH_4Cl and extracted with CH_2Cl_2. The organic phase was dried over anhydrous Na_2SO_4 and the solvent was evaporated to dryness under vacuum. The crude product was purified by flash chromatography using hexane/dichloromethane (60:40) as eluent to afford F-BODIPY **4b** as red solid (**0.40 g, 63 %**). Melting point (°C): 234-236. FTIR (ATR) (ν, cm^{-1}): 3108, 2214, 1699, 1678, 1558, 1534, 1413, 1386, 1260, 1101, 1086, 1069, 758. UV-Vis ($CHCl_3$) λ = 305, 316, 377, 506 nm. ^{1}H-NMR [400 MHz, $CDCl_3$] (δ, ppm): 10.05 (s, 1H, H-17), 7.96 (br, 2H, H-3), 7.91 (d, *J* = 8.4 Hz, 2H, H-15), 7.72 (ddd, *J* = 5.9, 3.8, 1.7 Hz, 4H, H-8, H-9), 7.60 (d, *J* = 8.4 Hz, 2H, H-14), 6.94 (d, *J* = 4.2 Hz, 2H, H-1), 6.57 (d, *J* = 4.2 Hz, 2H, H-2). ^{13}C-NMR [100 MHz, $CDCl_3$] (δ, ppm): 191.5 (C-17), 146.2 (C-7), 144.6 (C-3), 135.9 (C-16), 134.7 (C-6), 134.3 (C-10), 133.2 (C-5), 132.4 (C-8), 131.9 (C-9), 131.4 (C-1), 130.7 (C-14), 129.8 (C-15), 125.4 (C-13), 118.9 (C-2), 92.1 (C-11), 91.2 (C-12). ^{11}B-NMR [128.3 MHz, $CDCl_3$] (δ, ppm): -0.33 (t, *J* = 28.5 Hz).^{19}F-NMR [282.4 MHz,

$CDCl_3$] (δ, ppm): -144.99 (q, *J* = 28.5 Hz). HRMS calculated for *m/z* $C_{24}H_{15}BF_2N_2O+H^+$ 397.1324, found 397.1321.

Crystal Data

Single crystal X-ray diffraction analysis of **4a-b** were performed on an Enraf Nonious Kappa-CCD (λ MoK_α= 0.71073 Å, graphite monochromator, T= 298 K-CCD) at 293 (2) K. All reflection data set were corrected for Lorentz and polarization effects. The crystals were mounted on conventional MicroLoops™. The first structure solution was obtained using the SHELXS-97 [15] or SIR [27] programs and then SHELXL-97 [15] program was applied for refinement and output data. All software manipulations were done under the WinGX [28] environment program set. All heavy atoms were found by Fourier map difference and refined anisotropically. The programs Mercury [16] and ORTEP-3 [29] were used to prepare artwork representations. Table 2 lists the crystallographic data for compounds **4a-b**.

Compound	**4a**	**4b**
Empirical formula	$C_{22}H_{13}BF_2N_2OS$	$C_{24}H_{15}BF_2N_2O$
Formula weight	402.21	396.16
Space group	P -1	P-1
Crystal system	Triclinic	Triclinic
a (Å)	6.1941 (5)	7.7466 (4)
b (Å)	11.0277 (9)	7.9869 (4)
c (Å)	14.9923 (12)	16.3598 (9)
α (°)	68.625 (3)	99.532 (2)
β (°)	85.063 (3)	97.223 (3)
γ (°)	75.119 (4)	105.005 (2)
Volume ($Å^3$)	921.62 (13)	948.97 (9)
Z	2	2
Crystal size	0.75 x 0.65 x 0.25	0.66 x 0.52 x 0.35
Temperature	293 (2)	293 (2)
δ (mg/m^3)	1.449	1.387
θ range for data collection	2.918 to 27.517	3.219 to 27.953
Index ranges	$-7 \le h \le 8$ $-14 \le k \le 13$ $-19 \le l \le 19$	$-10 \le h \le 6$ $-10 \le k \le 10$ $-21 \le l \le 20$
Reflections collected	10213	12598
Data/Restraints/Parameters	4028/0/262	4288/0/275
Final R indices	R_1 = 0.0423 wR_2 = 0.1035	R_1 = 0.0534 wR_2 = 0.1223

R indices (*all data*)	R_1 = 0.0673 wR_2 = 0.1265	R_1 = 0.1432 wR_2 = 0.1535

Table 2. Crystallographic data for F-BODIPYs **4a-b**

Absorption Spectroscopy

The spectroscopic properties of F-BODIPYs **4a-b** were determined on solutions prepared by dissolving crystalline compounds in $CHCl_3$. Stock solutions (1 x 10^{-3} M) were prepared and diluted to appropriate concentrations for determination of absorbance. The UV-Vis spectra were recorded in a Thermo Scientific Evolution diode array UV-Vis spectrophotometer.

Computational Methods

The periodic systems were optimized using the program Dmol3, contained in the Materials Studio 8 (MS8) suite [26]. Functional PW91 was employed through all the calculations, with the DNP+ basis set [21]. Density of states (DOS) and band structure diagrams were computed using the Cambride Serial Total Energy Package (CASTEP code), a plane-wave pseudopotential method based on density functional theory for calculation of the total energy of large systems, bundled in MS8. The GGA functional PW91 was employed for all CASTEP computations, with fine convergence criteria and norm-conserving pseudopotentials. Natural Bonding Orbitals (NBO) were computed at the HF/6-31G(d) level using the Gaussian '09 software [30]. For Atoms-in-Molecules topological analysis of the electron density, the AIMALL software was employed [31]. The input for these calculations was the electron density derived during NBO computation.

Acknowledgements

E.X.-F. (**211329**) thanks CONACYT for scholarship. Thanks are due to DGAPA-ICN UNAM for the postdoctoral fellowship granted to R. Arcos-Ramos. The authors also would thank to CONACYT and DGAPA for financial support.

Appendix A. Supplementary Materials

Experimental procedures for the intermediates **1a-b** and **2a-b** are available in the supporting information file with the corresponding ^{1}H, ^{13}C, ^{11}B and ^{19}F NMR spectral data associated to this paper. CCDC numbers 1422479 (**4a**) and 1429950 (**4b**) contain the supplementary crystallographic data for this paper. These data can be obtained free of charge via http://www.ccdc.cam.ac.uk/conts/retrieving.html (or from the Cambridge Crystallographic Data Centre, 12, Union Road, Cambridge CB2 1EZ, UK; fax: +44 1223 336033).

References

[1] (a) H. Lu, J. Mack, Y. Yang, Z. Shen, Chem. Soc. Rev. 43 (2014) 4778-4823.

(b) V. Lakshmi, M. Rajeswara Rao, M. Ravinkanth, Org. Biomol. Chem., 13 (2015) 2501-2517.

(c) M.E. El-Khouly, S. Fukuzumi, F. D'Souza, ChemPhysChem 15 (2014) 30-47.

(d) A. Loudet and K. Burgess, Chem. Soc. Rev. 107 (2007) 4891-4932.

[2] (a) F. Bergstom, I. Mikhalyov, P. Hagglof, R. Wortmann, T. Ny, L.B.-A. Johansson, J. Am. Chem. Soc. 124 (2002) 196-204.

(b) A. Aharoni, L. Weiner, A. Lewis, M. Ottolenghi, M. Sheves, J. Am. Chem. Soc. 123 (2001) 6612-6616.

[3] T.A. Golovkova, D.V. Kozlov, D.C. Neckers, J. Org. Chem. 70 (2005) 5545-5549.

[4] C.N. Baki, E.U. Akkaya, J. Org. Chem. 66 (2001) 1512-1513.

[5] A. Kamikaew, S.H. Lim, H.B. Lee, L.V. Kiew, L.Y. Chung, K. Burgess, Chem. Soc. Rev. 42 (2013) 77-88.

[6] Y. Kajiwara, A. Nagai, Y. Chujo, Bull. Chem. Soc. Jpn. 84 (2011) 471-472.

[7] (a) G. Ulrich, C. Goze, M. Guardigli, A. Roda, R. Ziessel, Angew. Chem. Int. Ed. 44 (2005) 3694-3698.

(b) R. Ziessel, G. Ulrich, A. Harriman, New J. Chem. 31 (2007) 496-501.

(c) G. Ulrich, R. Ziessel, A. Harriman, Angew. Chem. Int. Ed. 47 (2008) 1184-1201.

(d) L. Luo, D. Wu, W. Li, S. Zhang, Y. Ma, S. Yan, J. Jou, Org. Lett. 16 (2014) 6080-6083.

[8] T.V. Goud, A. Tutar, J.F. Biellmann, Tetrahedron 62 (2006) 5084-5091.

[9] V. Leen, P. Yuan, L. Wang, N. Boens, W. Dehaen, Org. Lett. 14 (2012) 6150-6153.

[10] (a) R. Misra, B. Dhokole, T. Jadhav, S.M. Mobin, Dalton. Trans. 43 (2014) 4854-4861.

(b) B. Dhokale, T. Jadhav, S.M. Mobin, R. Misra, J. Org. Chem. 80 (2015) 8018-8025.

[11] (a) C. Katan, M. Charlot, O. Mongin, C. Le Droumaguet, V. Jovikov, F. Terenzian, E. Badaeva, S. Tretiak, M. Blanchard-Desce, J. Phys. Chem. B. 114 (2010) 3152-3169.

(b) L.M. Yagupolskii, V.N. Petrik, Y.L. Slominskii, Tetrahedron Lett. 43 (2000) 3957-3959.

(c) R.L. Hinman, J. Org. Chem. 25 (1960) 1775-1778.

(d) J. Bañuelos, V. Martin, C.F. Azael Gomez-Duran, I.J. Arroyo Cordoba, E. Peña Cabrera, I. Garcia Moreno, M.E. Perez-Ojeda, T. Arbeloa, I.L. Arbeloa, Chem. Eur. J. 17 (2011) 7261-7270.

[12] (a) L.Li, B. Nguyen, K. Burgess, Bioorg. Med. Chem. Lett. 18 (2008) 3112-3115.

(b) K. Umezawa, Y. Nakamura, H. Makino, D. Citterio, K. Suzuki, J. Am. Chem. Soc. 130 (2008) 1550-1551.

(c) L.N. Sobenina, A.M. Vasiltsov, O.V. Petrovam K.B. Petrushenko, I.A. Ushakov, G. Clavier, R. Meallet-Renault, A.I. Mikhaleva, B.A. Trofimov, Org. Lett. 13 (2011) 2524-2527.

(d) S. Choi, J. Bouffard, Y. Kim, Chem. Sci., 5 (2014) 751-755.

[13] (a) J.M. You, H. Jeong, H. Seo, S. Jeon, Sensors and Actuators B 146 (2010) 160-164.

(b) F. Fungo, L.A. Otero, L. Sereno, J.J. Silber, E.N. Durantini, J. Mater. Chem. 10 (2000) 645-650.

(c) T. Khan, R.S. Pissurlenkar, M.S. Shaik, M. Ravinkanth, J. Organomet. Chem. 697 (2012) 65-73.

(d) Y. Fu, Q. He, D. Zhu, Y. Wang, Y. Gao, H. Cao, J. Cheng, Chem. Commun. 49 (2013) 11266-11268.

[14] (a) K. Sonogashira, Y. Thoda, N. Hagihara, Tetrahedron Lett. 16 (1975) 4467-4470.

(b) S. Thorand, N. Krauze, J. Org. Chem., 63 (1998) 8551-8553.

(c) R. Arcos-Ramos, B. Rodriguez-Molina, E. Gonzalez-Rodriguez, P.I. Ramirez-Montes, M.E. Ochoa, R. Santillan, N. Farfan, M.A. Garcia-Garibay, RSC Adv. 5 (2015) 55201-55208.

(d) R. Arcos-Ramos, B. Rodriguez-Molina, M. Romero, J.M. Mendez-Stivalet, M.E. Ochoa, P.I. Ramirez-Montes, R. Santillan, M.A. Garcia-Garibay, N. Farfan, J. Org. Chem. 77 (2012) 6887-6894.

[15] G.M. Sheldrick, Acta Crystallogr. A64 (2008) 112-122.

[16] C.F. Macrae, P.R. Edgington, P. McCabe, E. Pidcock, G.P. Shields, R. Taylor, M. Towler, J. van de Streek, J. Appl. Crystallogr., 39 (2006) 453-457.

[17] (a) S. Rihn, P. Retailleau, N. Bugsaliewicz, A. De Nicola, R. Ziessel, Tetrahedron Lett. 50 (2009) 7008-7013.

(b) H.L. Kee, C. Kirmaier, L.H. Yu, P. Thamyongkit, W.J. Youngblood, M.E. Calder, L. Ramos, B.C. Noll, D.F. Bocian, W.R. Scheidt, R.R. Birge, J.S. Lindsey, D.J. Holten, J. Phys. Chem. B. 109 (2005) 20433-20443.

[18] (a) B. Dhokale, P. Gautam, S.M. Mobin, R. Misra, Dalton. Trans. 42 (2013) 1512-1518.

(b) C.F.-A- Gomez-Duran, R. Hu, G. Feng, T. Li, F. Bu, M. Arseneault, B. Liu, E. Peña-Cabrera, B.Z. Tang, ACS Appl. Mater Interfaces 7 (2015) 15168-15176.

(c) C. Yu, L. Jiao, H. Yin, J. Zhou, W. Pang, Y. Wu, Z. Wang, G. Yang, E. Hao, Eur. J. Org. Chem. 28 (2011) 5460-5468.

[19] (a) S.K. Sarkar, P. Thilagar, Chem. Commun. 49 (2013) 8558-8560.

(b) D. Collado, J. Casado, S. Rodríguez-González, J.T. López-Navarrete, R. Suau, T.M. Pappenfus, M.M. Raposo, Chem. Eur. J. 17 (2011) 498-507.

[20] H. Guo, Y. Jing, X. Yuan, S. Ji, J. Zhao, X. Li, Y. Kan, Org. Biomol. Chem. 9 (2011) 3844-3853.

[21] For a study on the relative performance of numerical vs. analytical orbitals in DFT computations, please refer to: B. Delley, Chem. Phys. 110 (1986) 329-338.

[22] A. Klamt, G. Schüürmann, J. Chem. Soc., Perkin Trans. 2 (1993) 799-805.

[23] R. Bader, Chem. Rev. 91 (1991) 893-928.

[24] K. Weinhold, C. R. Landis, Chem. Educ. Res. Pract. Eur. 2 (2001) 91-104.

[25] R. Misra, B. Dhokale, T. Jadhav, S.M. Mobin, New. J. Chem. 38 (2014) 3579-3585.

[26] Computational results obtained using software programs from Dassault Systèmes Biovia Corp. Calculations were performed with the CASTEP code, and graphical displays generated with Materials Studio.

[27] A. Altomare, M.C. Burla, M. Camalli, A.G. Moliterni, G. Polidori and R. Spagna. J. Appl. Cryst. 32 (1999) 115-119.

[28] L.J. Farrugia, J. Appl. Crystallogr. 32 (1999) 837-838.

[29] L.J. Farrugia, J. Appl. Crystallogr. 30 (1997) 565.

[30] Gaussian 09, Revision D.01, M.J. Frisch, G.W. Trucks, H.B. Schlegel, G.E. Scuseria, M.A. Robb, J.R. Cheeseman, G. Sacalmani, V. Barone, B. Menucci, G.A. Petersson, H. Nakatsuji, M. Caricato, X. Li, H.P. Hratchian, A.F. Izmaylov, J. Bloino, G. Zheng, J.L. Sonnenberg, M. Hada, M. Ehara, K. Toyota, R. Fukuda, J. Hasegawa, M. Ishida, T. Nakajima, Y. Honda, O. Kitao, H. Nakai, T. Vreven, J.A. Montgomery, J.E. Peralta, F. Ogliaro, M. Bearpak, J.J. Heyd, E. Brothers, K.N. Kudin, V.N. Staroverov, R. Kobayashi, J. Normand, K. Raghavachari, A. Rendell, J.C. Burant, S.S. Iyengar, J. Tomasi, M. Cossi, N. Rega, J.M. Millam, M. Klene, J.E. Knox, J.B. Cross, V. Bakken, C. Adamo, J. Jaramillo, R. Gomperts, R.E. Stratmann, O. Yazyev, A.J. Austin, R. Cammi, C. Pomelli, J.W. Ochterski, R.L. Martin, K. Morokuma, V.G. Zakrzewsli, G.A. Voth, P. Salvador, J.J. Dannenberg, S. Dapprich, A.D. Daniels, Ö. Farkas, J.B. Foresman, J.V. Ortiz, J Ciolowski, J. Fox, Gaussian 09, Revisions, A.02, Gaussian, Inc., Wallingford, CT, 2009.

[31] AIMAll (Version 15.09.27), T. A. Keith, TK Gristmill Software, Overland Park KS, USA, 2015.

Highlights

1. Molecular crystals were solved in the P-1 space group.
2. UV-Vis excitations have been computed and correlated with the experiments.
3. The electron density for each unit cell was analyzed by QTAIM.
4. NBO mapping of intermolecular orbital overlap was derived.
5. Density of states was derived through CASTEP analysis.